

Evidence for Non-Hydrostatic Gas from the Cluster X-ray to Lensing Mass Ratio

A. Mahdavi¹, H. Hoekstra^{1,2}, A. Babul¹, J. P. Henry³

¹*University of Victoria, Elliott Building, 3800 Finnerty Road, Victoria, BC V8P 5C2 Canada*

²*Alfred P. Sloan Research Fellow*

³*Institute for Astronomy, University of Hawaii, 2680 Woodlawn Drive, Honolulu, HI 96822*

26 October 2021

ABSTRACT

Using a uniform analysis procedure, we measure spatially resolved weak gravitational lensing and hydrostatic X-ray masses for a sample of 18 clusters of galaxies. We find a radial trend in the X-ray to lensing mass ratio: at r_{2500} we obtain a ratio $M_X/M_L = 1.03 \pm 0.07$ which decreases to $M_X/M_L = 0.78 \pm 0.09$ at r_{500} . This difference is significant at 3σ once we account for correlations between the measurements. We show that correcting the lensing mass for excess correlated structure outside the virial radius slightly reduces, but does not eliminate this trend. An X-ray mass underestimate, perhaps due to nonthermal pressure support, can explain the residual trend. The trend is not correlated with the presence or absence of a cool core. We also examine the cluster gas fraction f_{gas} and find no correlation with M_L , an important result for techniques that aim to determine cosmological parameters using f_{gas} .

Key words: Gravitational lensing - X-rays: galaxies: clusters - dark matter - galaxies: clusters: general

1 INTRODUCTION

Rich clusters of galaxies host the most massive collapsed dark matter halos. The X-ray emitting intracluster medium (ICM) bound to this halo can be a useful tracer of the dark matter content of the cluster. Under the assumption of hydrostatic equilibrium the gradients of the gas pressure P and total gravitational potential Φ are related by the simple differential equation

$$\nabla P = \rho_g \nabla \Phi \quad (1)$$

where ρ_g is the gas density. The hydrostatic method is in principle powerful, because spatially resolved measurements of the gas pressure can constrain the shape of the halo and hence yield useful limits on fundamental dark matter properties and cosmology.

In reality, we do not know the reliability of hydrostatic mass estimates. Not only are merging clusters of galaxies in a nonhydrostatic state, but the plasma in many apparently relaxed systems may be affected by additional nonequilibrium processes, which serve to boost P and hence cause an underestimate of the cluster mass from X-ray observations of the thermal bremsstrahlung emission. In early hydrodynamic N-body simulations, Evrard (1990) found the first signs of this underestimate, attributing it to incomplete thermalization of the ICM. More recent N-body work has shown that energy input from active galactic nuclei, pressure sup-

port from turbulence and residual bulk motions, and variations in the merging history may contribute substantially to this systematic bias (Dolag et al. 2005; Faltenbacher et al. 2005; Rasia et al. 2006; Nagai et al. 2007; Ameglio et al. 2007). Importantly, constraints on dark energy from the cluster mass function are highly sensitive to intrinsic scatter and systematic error in the mass-observable relation (Lima & Hu 2005); the scatter also significantly influences the normalization of the primordial fluctuation spectrum σ_8 (Balogh et al. 2006).

Comparison with independent methods can provide a powerful means of checking the reliability of X-ray mass measurements. Here we focus on comparison of hydrostatic X-ray masses with those derived from weak gravitational lensing. Unlike the hydrostatic method, gravitational lensing does not require assumptions regarding the dynamical state of the cluster. Early work comparing lensing and X-ray masses showed that while strong gravitational lensing masses in merging clusters sometimes exceeded X-ray masses by factors of $\approx 1.5 - 2$, weak lensing masses measured at larger radii are consistent with the X-ray data to within $\approx 20\%$ (Miralda-Escude & Babul 1995; Squires et al. 1996; Allen et al. 1996; Squires et al. 1997; Allen 1998). This picture is supported by subsequent ground- and space-based observations of relaxed and merging clusters, albeit with fairly large uncertainties

(Allen et al. 2002; Smith et al. 2001; Hoekstra et al. 2002; Ettori & Lombardi 2003; Cypriano et al. 2004; Hicks et al. 2006).

Only recently has data with the accuracy required to carry out a systematic comparison of larger samples of hydrostatic and lensing masses become available. Recent studies, however, are apparently in conflict. For a sample of 30 clusters, Pedersen & Dahle (2007) report a 30% excess in the normalization of lensing mass-temperature (M-T) relative to the X-ray value within¹ r_{500} . However, Hoekstra (2007) using 20 clusters which also form the basis of this paper, report no significant excess in the M-T normalization at r_{2500} .

To study the difference in X-ray and lensing masses in greater detail, we present a sample of 18 clusters—the largest yet with accurate spatially resolved hydrostatic as well as weak lensing masses. In our study, we take particular care to account for possible systematic effects in the lensing and X-ray measurement process. Our data support a picture in which the lensing excess is negligible at r_{2500} , but increases at larger radii. In Section 2 we discuss our data reduction procedure; in Section 3 we discuss the trend in the $M_X - M_L$ relation; in Section 4 we account for potential biases; in Section 5 we consider trends in the gas fraction; and in Section 6 we conclude. We assume $H_0 = 70$ km s⁻¹ Mpc⁻¹, $\Omega_M = 0.3$, and $\Omega_\Lambda = 0.7$.

2 DATA

2.1 Lensing data

The clusters in our sample were drawn from Hoekstra (2007), which contains a weak lensing analysis of CFH12k data from the Canada-France-Hawaii Telescope. We refer interested readers to Hoekstra (2007) for details of the data reduction and weak lensing analysis procedure. The shear measurements discussed in this paper are identical to Hoekstra (2007), but here we present updated values for the masses. The changes are due purely to the fact that Hoekstra (2007) used the Hubble Deep Field (HDF) redshift distribution (Fernández-Soto et al. 1999), which is based on data taken within a much smaller field than the Ilbert et al. (2006) study, based on the CFHT Legacy Survey data. The conversion of the lensing signal into a physical mass estimate depends directly on the source redshift distribution. This dependence is quantified by the parameter $\beta_{\text{lens}} = \max[0, D_{ls}/D_s]$, where D_{ls} and D_s are the angular diameter distances between the lens and the source, and the observer and the source. We note that β_{lens} is an important parameter because it is degenerate with the projected cluster mass.

We calculate the new β_{lens} values using the photometric redshift distributions derived by Ilbert et al. (2006). The resulting values are listed in Table 1. The mean redshift derived by Ilbert et al. (2006) is higher (also see Benjamin et al. 2007) resulting in a $\sim 10\%$ reduction in the inferred cluster mass compared to those in Hoekstra (2007).

¹ For a cluster at redshift z , the overdensity radius r_Δ is the radius within which the mean matter density is Δ times the critical density of the universe at redshift z . M_Δ is the mass within that radius.

As the Ilbert et al. (2006) results are based on four independent pointings, we can also examine the field-to-field variation in β_{lens} . We find this to be a negligible effect, with a dispersion of only a 1–2 percent. Although systematic biases may still be present, the results from Ilbert et al. (2006) provide a significant improvement over previous studies. Consequently, we expect that the current uncertainty in the source redshift distribution affects our mass estimates only at the few percent level.

We base our lensing masses on the aperture mass estimates (for details see the discussion in §3.5 in Hoekstra 2007). This approach has the advantage that it is practically model independent. Additionally, as the mass estimate relies only on shear measurements at large radii, contamination by cluster members is minimal. Hoekstra (2007) removed galaxies that lie on the cluster red-sequence and boosted the signal based on excess number counts of galaxies. As an extreme scenario we omitted those corrections and found that the lensing masses change by only a few percent at most. Hence our masses are robust against contamination by cluster members at the percent level.

The weak lensing signal, however, only provides a direct estimate of the *projected* mass. To calculate 3D masses (such as M_{2500} , M_{1000} , and M_{500}) from the model-independent 2D aperture masses we project and renormalize a density profile of the form $\rho_{\text{tot}}(r) \propto r^{-1}(r_{200} + cr)^{-2}$ (Navarro et al. 1997). The relationship between the concentration c and the virial mass is fixed at $c \propto M_{200}^{-0.14}/(1+z)$ from numerical simulations (Bullock et al. 2001). Hence, the deprojection itself, though well motivated based on numerical simulations, is model dependent.

2.2 X-ray data

Data for 18 of the 20 clusters in Hoekstra (2007) are available in the Chandra X-ray Observatory (CXO) public archive. We analyze and fit these data using the Joint Analysis of Cluster Observations (JACO) package (Mahdavi et al. 2007). The reduction procedure follows the detailed description in Mahdavi et al. (2007), except as discussed below. We briefly summarize the procedure here. We reprocess the raw CXO data with CALDB 3.3, including the charge transfer inefficiency correction for ACIS-I data. To remove the particle background, we subtract the appropriate blank-sky observation renormalized to match 9–12 keV count rates in the most source-free region of the data. We examine the residual spectra in 9–12 keV energy range for each cluster to ensure that the particle background is cleanly subtracted.

We then extract spectra in circular annuli centered on the X-ray surface brightness peak, masking any detected non-cluster sources. The residual diffuse astrophysical background is fit as an additive component as described in the analysis below.

The spectra are fit with a projected 3D cluster model. We begin with a mass profile consisting of an NFW dark matter distribution and a gas density of the form

$$\rho_g = \sum_{i=1}^{N_\beta} \rho_i (1 + r^2/r_{x,i}^2)^{-3\beta_i/2}, \quad (2)$$

where $r_{x,i}$ are the core radii and β_i are the slopes of the N_β

Table 1. Weak-Lensing Measurements

Cluster	z	β_{lens}	M_{2500}	r_{2500}	M_{1000}	r_{1000}	M_{500}	r_{500}
Abell 68	0.255	0.504	2.56 ± 0.60	0.52	4.51 ± 1.30	0.85	6.64 ± 2.44	1.22
Abell 209	0.206	0.627	1.89 ± 0.67	0.48	4.40 ± 1.61	0.86	7.14 ± 1.93	1.27
Abell 267	0.230	0.522	2.14 ± 0.39	0.49	3.70 ± 1.10	0.80	6.29 ± 1.93	1.21
Abell 370	0.375	0.412	3.86 ± 0.66	0.57	7.79 ± 1.86	0.97	13.27 ± 3.40	1.47
Abell 383	0.187	0.641	0.76 ± 0.33	0.35	2.29 ± 1.04	0.69	4.49 ± 1.96	1.09
Abell 963	0.206	0.592	1.39 ± 0.41	0.43	2.50 ± 0.90	0.71	4.16 ± 1.54	1.06
Abell 1689	0.183	0.639	4.74 ± 0.77	0.65	9.11 ± 1.31	1.10	14.29 ± 2.40	1.61
Abell 1763	0.223	0.574	2.93 ± 0.59	0.55	5.51 ± 1.43	0.92	10.47 ± 2.84	1.43
Abell 2218	0.176	0.644	2.66 ± 0.64	0.54	4.59 ± 1.10	0.88	6.10 ± 1.64	1.22
Abell 2219	0.226	0.562	3.10 ± 0.60	0.56	6.81 ± 1.79	0.98	10.27 ± 2.31	1.42
Abell 2390	0.228	0.586	3.04 ± 0.59	0.55	6.29 ± 1.43	0.96	8.79 ± 1.99	1.35
CL 0024.0+1652	0.390	0.379	3.16 ± 0.63	0.53	5.90 ± 1.66	0.88	9.87 ± 3.36	1.32
MS 0015.9+1609	0.547	0.267	3.74 ± 0.87	0.53	11.30 ± 3.07	1.03	19.51 ± 5.77	1.56
MS 0906.5+1110	0.170	0.674	1.99 ± 0.57	0.49	4.87 ± 1.54	0.90	9.46 ± 2.06	1.41
MS 1358.1+6245	0.329	0.447	2.23 ± 0.51	0.48	4.11 ± 1.33	0.80	6.64 ± 2.66	1.18
MS 1455.0+2232	0.257	0.564	1.51 ± 0.36	0.43	3.11 ± 1.00	0.75	4.83 ± 1.70	1.09
MS 1512.4+3647	0.373	0.434	0.74 ± 0.36	0.33	1.43 ± 0.74	0.55	2.94 ± 2.11	0.89
MS 1621.5+2640	0.428	0.368	2.03 ± 0.87	0.45	5.40 ± 1.80	0.84	7.64 ± 2.74	1.19

All masses are in units of $10^{14} M_{\odot}$; all radii are in units of Mpc; z is the redshift of the clusters, and β_{lens} is a measure of the source redshift distribution.

independent “ β -model gas distributions. We assume that the gas metallicity is of the form

$$Z(r) = Z_0(1 + r^2/r_z^2)^{-3\beta_Z/2}. \quad (3)$$

where Z_0 is the central metallicity, and r_Z and β_Z describe the metallicity profile.

The 3D temperature profile is calculated self-consistently using the equation of hydrostatic equilibrium:

$$T(r) = \frac{1}{\rho_g} \left(\rho_{100} T_{100} + \frac{\mu m_p}{k} \int_r^{r_{100}} \frac{GM\rho_g}{r'^2} dr' \right) \quad (4)$$

where M is the total mass profile, μ is the mean molecular weight, m_p is the proton mass, r_{100} is the radius at which the gas distribution is truncated, ρ_{100} is the gas density at the truncation radius, and T_{100} is the temperature at that radius. We project the resulting 3D emissivity along the line of sight, absorb it by the galactic hydrogen column as fixed by Dickey & Lockman (1990), convolve the result by the instrumental response, and compare with the measured spectra using a χ^2 statistic. A standard MEKAL plasma with variable abundance serves as the spectral model.

The fitting procedure begins with a single β model fit ($N_{\beta} = 1$); if this yields a poor fit, one or two β model components are added until the fit becomes acceptable. In two cases (Abell 1689 and Abell 2390) we could only obtain a good fit by also excising the central 70 kpc, as Vikhlinin et al. (2006) suggest. Other simultaneously fit parameters are the gas metallicity profile (3 free parameters), the dark matter profile (2 free parameters), the normalizations of the diffuse astrophysical backgrounds (3 free parameters), and the temperature at the truncation radius T_{100} . The astrophysical backgrounds are modeled as a power law with fixed slope 1.4 and free normalization (to model unresolved background AGN), and a unredshifted thermal plasma with free normalization and $T < 0.5$ keV (to model the local soft X-ray background).

Accounting for the covariance of all measurable param-

eters, proper treatment of the truncation of the gas distribution, simultaneous fitting of the background, and the absence of subjectively weighted 2D temperatures (Vikhlinin 2006) are unique features of the JACO code and are described in detail in Mahdavi et al. (2007).

The measured masses are robust to variations of the gas truncation radius; varying this radius between r_{200} and r_{500} yields a 3% random variation in the measured masses. T_{100} was often poorly constrained (only lower limits were possible with lower quality data). The JACO error analysis routines include this uncertainty in the final masses.

The resulting total gravitating masses are listed in Table 2. In Figure 1 we compare these masses with the values reported for the same Chandra observations in LaRoque et al. (2006) and Allen et al. (2007). We find that our masses on the average in excellent agreement with the two samples, with the LaRoque et al. (2006) values being somewhat lower, and the Allen et al. (2007) values somewhat higher, than ours.

3 THE M_X/M_L RATIO

3.1 A Radial Trend

We examine the relationship between the X-ray and lensing masses at each density contrast using a simple constant of proportionality:

$$M_{\Delta,X} = a_{\Delta} M_{\Delta,L} \quad (5)$$

Both M_X and M_L are measured within the weak-lensing derived value of r_{Δ} . To estimate a_{Δ} properly, we minimize a modified χ^2 statistic appropriately weighted for errors in both coordinates (Press et al. 1992):

$$\chi^2 = \sum \frac{(M_{\Delta,X} - a_{\Delta} M_{\Delta,L})^2}{\sigma_{\Delta,X}^2 + a_{\Delta}^2 \sigma_{\Delta,L}^2} \quad (6)$$

Table 2. X-ray Measurements

Cluster	N_β	χ^2/ν	M_{2500}	M_{1000}	M_{500}	f_{2500}	r_{cool}	Extrapolated
Abell 68	1	98/98	3.18 ± 1.96	4.98 ± 4.10	6.63 ± 6.15	0.09 ± 0.06	...	1000,500
Abell 209	1	184/179	2.00 ± 0.45	3.97 ± 1.77	5.91 ± 2.98	0.12 ± 0.03	...	1000,500
Abell 267	1	317/303	2.27 ± 0.31	4.08 ± 0.98	6.26 ± 2.05	0.10 ± 0.01	0.030 ± 0.030	500
Abell 370	1	915/804	2.99 ± 0.24	5.81 ± 1.47	9.22 ± 1.28	0.12 ± 0.01	...	500
Abell 383	3	402/366	1.22 ± 0.06	3.04 ± 0.65	5.03 ± 1.34	0.10 ± 0.01	0.114 ± 0.014	500
Abell 963	3	1129/1071	1.92 ± 0.21	3.24 ± 0.52	4.20 ± 1.64	0.11 ± 0.01	0.079 ± 0.008	1000,500
Abell 1689	3	1065/917	4.47 ± 0.89	7.40 ± 2.32	9.86 ± 3.23	0.12 ± 0.02	0.082 ± 0.015	500
Abell 1763	1	440/419	2.56 ± 0.17	4.78 ± 0.50	7.68 ± 1.11	0.12 ± 0.01	...	500
Abell 2218	2	790/745	2.43 ± 0.49	2.89 ± 0.89	5.99 ± 2.33	0.11 ± 0.02	...	1000,500
Abell 2219	1	2272/2249	4.62 ± 0.47	10.88 ± 3.18	17.32 ± 6.50	0.11 ± 0.01	...	1000,500
Abell 2390	3	3663/3341	3.75 ± 0.31	7.53 ± 1.09	10.87 ± 2.09	0.14 ± 0.01	0.099 ± 0.009	1000,500
CL 0024.0+1652	1	165/127	1.86 ± 0.34	4.87 ± 0.74	9.92 ± 9.90	0.09 ± 0.02	0.073 ± 0.023	1000,500
MS 0015.9+1609	1	632/580	2.67 ± 0.19	6.52 ± 1.09	10.28 ± 2.42	0.21 ± 0.01
MS 0906.5+1110	2	587/549	1.59 ± 0.19	2.49 ± 0.45	3.23 ± 0.73	0.11 ± 0.01	0.030 ± 0.030	500
MS 1358.1+6245	2	752/675	2.83 ± 0.78	6.31 ± 2.81	11.08 ± 6.33	0.09 ± 0.02	0.077 ± 0.012	500
MS 1455.0+2232	3	1869/1685	1.40 ± 0.04	2.25 ± 0.10	2.96 ± 0.16	0.15 ± 0.01	0.123 ± 0.010	...
MS 1512.4+3647	1	254/243	0.69 ± 0.13	1.15 ± 0.28	1.74 ± 0.44	0.12 ± 0.02	0.095 ± 0.028	...
MS 1621.5+2640	1	237/255	1.54 ± 0.21	3.61 ± 0.54	5.43 ± 1.22	0.13 ± 0.02

All masses at density contrast Δ are in units of $10^{14}M_\odot$ and measured within the lensing radius r_Δ as listed in Table 1. N_β is the number of β -models required to achieve a good fit; χ^2/ν is the ratio of the χ^2 statistic to the number of degrees of freedom ν for the simultaneous fit to all spectra in all annuli; all masses are in units of $10^{14}M_\odot$. The cumulative gas fraction f_{2500} is the ratio of the gas mass to the total mass at r_{2500} ; r_{cool} is the radius (in units of Mpc) within which the isobaric cooling time is less than the age of the universe at the redshift of the cluster. Also shown are the density contrasts at which the masses had to be extrapolated beyond the available field-of-view.

This formulation implies no intrinsic scatter in the data, an assumption we validate below. We derive errors in a_Δ by locating the values at which $\chi^2 - \chi^2_{\text{min}} = 1$, which correspond to the 68% confidence interval.

The results appear in Figure 2. The simple one-parameter fit provides a good description of the relationship between M_X and M_L at all radii, and a clear trend is always present. The goodness-of-fit figure $\chi^2/\nu = 16/17$, $11/17$, and $14/17$ for masses measured within r_{2500} , r_{1000} , and r_{500} , respectively. Therefore, there is no evidence of intrinsic scatter in the $M_X - M_L$ relation. All scatter can be explained by the statistical error.

We find $a_{2500} = 1.03 \pm 0.07$, $a_{1000} = 0.90 \pm 0.09$, and $a_{500} = 0.78 \pm 0.09$. The formal significance of the result is higher than it seems from the quoted errors, because the three slopes a_Δ are correlated and therefore cannot be compared directly as a function of Δ . This is because the masses at each radius are correlated with the masses at other radii. Wherever the X-ray masses are extrapolated (as shown in Table 2), they are highly correlated with $M_{2500,X}$; the lensing masses at all radii are highly correlated, because the aperture masses are derived by integrating over the tangential shear from the radius of interest out to large radius.

To properly evaluate the significance of the difference between a_{2500} and a_{500} , we employ a bootstrap procedure with, calculating $a_{2500} - a_{500}$ many times. The resulting distribution appears in Figure 3. We find that $a_{2500} - a_{500}$ follows a Gaussian distribution with a mean of 0.24 and a standard deviation of 0.08. Thus, the difference in the M_X/M_L ratios at r_{2500} and r_{500} is significant at the 3σ level. Using a Monte Carlo simulation of the bootstrap processes, we confirm that the error obtained in this way is unbiased and the ‘‘error on the error’’ is close to the expected value, $0.07/\sqrt{36} \approx 0.01$, or 16%.

3.2 Interpretation

The variation of this constant of proportionality a_Δ as a function of radius can yield useful constraints on cluster physics. This statistically significant gradient in M_X/M_L may be explained through an X-ray mass underestimate. For example, the cosmological N-body simulations discussed by Nagai et al. (2007) predict a low M_X/M_{true} on account of nonthermal pressure support in the ICM: effects such as residual bulk motions cause hydrostatic mass estimates to be biased low. Earlier studies based on simulations (e.g. Evrard 1990; Faltenbacher et al. 2005; Rasia et al. 2006; Hallman et al. 2006) support this conclusion. Nagai et al. (2007) find that, on the average, clusters at $z = 0$ exhibit little significant bias within r_{2500} (-0.12 ± 0.16). However, within r_{500} , the fractional bias is more significant (-0.16 ± 0.10). Assuming that weak gravitational lensing mass has been corrected for projection effects (see below), the direction and magnitude of the effect predicted by Nagai et al. (2007) at r_{500} would seem to match our observed trend (see Figure 4).

An independent check on this result is a comparison with previously reported normalization of the $M_L - T$ relation. At r_{2500} , Hoekstra (2007) finds consistency between the normalizations of the $M_L - T$ from CFHT data and the $M_X - T$ relation from Vikhlinin et al. (2006). On the other hand, at r_{500} Pedersen & Dahle (2007) finds the normalization to be high by $\approx 30\%$. These results are consistent with the trend we detect here.

If, as we suggest, incomplete thermalization of ICM is responsible for the X-ray mass underestimate, we should expect clusters with the most substructure to exhibit the greatest deviations from $M_X = M_L$ (e.g. Abell 781, Sehgal et al. 2008). Recent theoretical work has shown that it may be

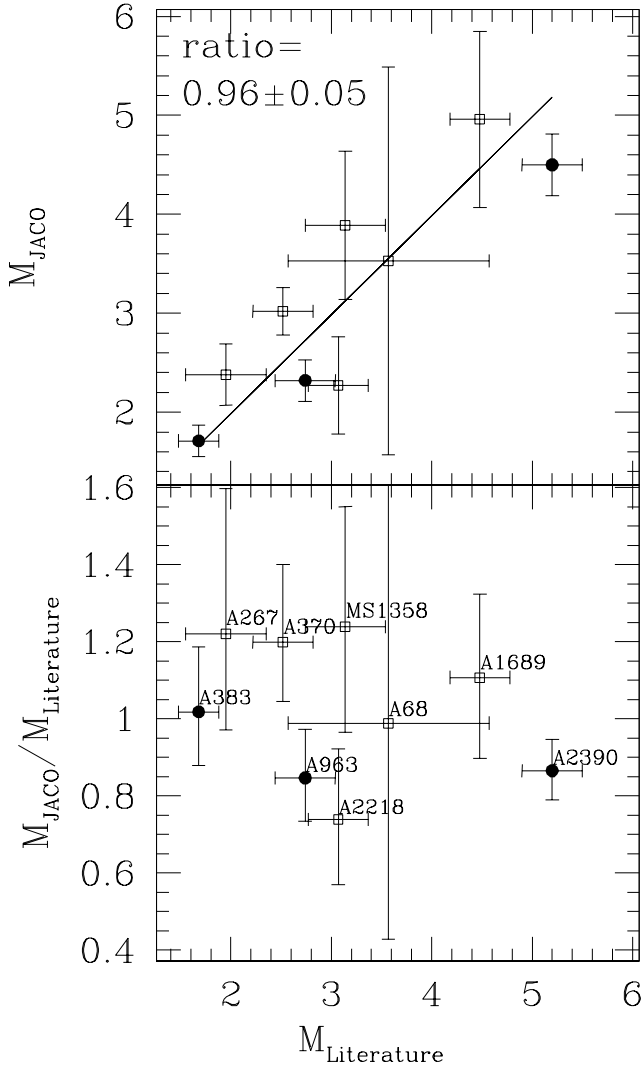


Figure 1. Comparison of JACO measurements of M_{2500} with other recent Chandra measurement for a subset of 9 clusters. All masses are in units of $10^{14} M_{\odot}$. The Abell 383, 963, and 2390 masses (filled points) are from Allen et al. (2007); the remainder (unfilled points) are from LaRoque et al. (2006). The JACO masses shown are estimated using X-ray data only, rather than calculated using the lensing values of r_{2500} as in Table 2.

possible to correct for the X-ray mass underestimate in this way (Jeltema et al. 2007). We look for such a trend in Figure 2 by dividing the clusters into cool core and non-cool core subsamples, under the hypothesis that clusters with cool cores are less likely to have experienced recent mergers. We find that there is no statistically significant difference in the $M_X - M_L$ relation for cool core and non-cool core clusters. This agrees with N-body simulations showing that the existence of a cool core is not a reliable predictor of the equilibrium state of a cluster of galaxies (e.g. Poole et al. 2006, 2007; Burns et al. 2007). More refined estimates of the level of substructure in each cluster are needed to evaluate the possibility of correcting for the X-ray underestimate. We will explore this avenue in a future paper.

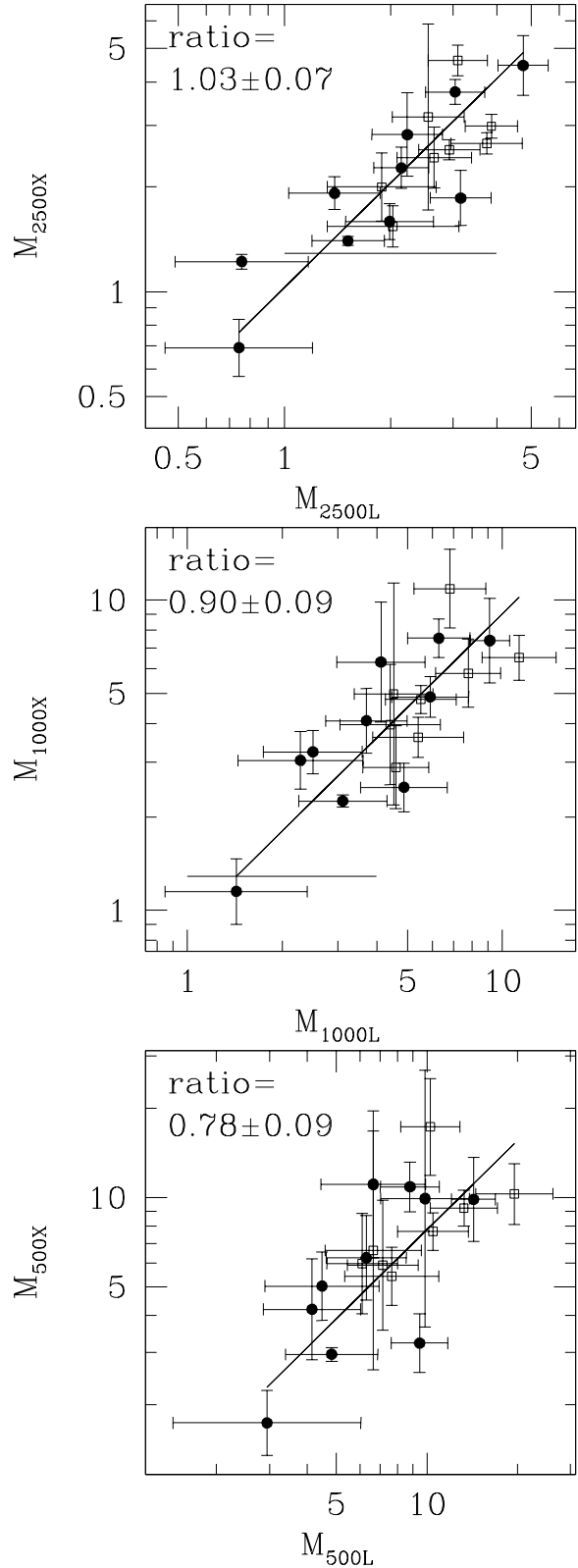


Figure 2. Ratio of the hydrostatic X-ray mass to the gravitational lensing mass, both measured within the lensing overdensity radii r_{2500} , r_{1000} , and r_{500} . All masses are in units of $10^{14} M_{\odot}$. There is significant trend of decreasing M_X/M_L with increasing radius. Filled circles and unfilled squares show systems with and without cool cores, respectively (we define non-cool core clusters as those where the cooling time is nowhere smaller than the age of the universe at the redshift of the cluster).

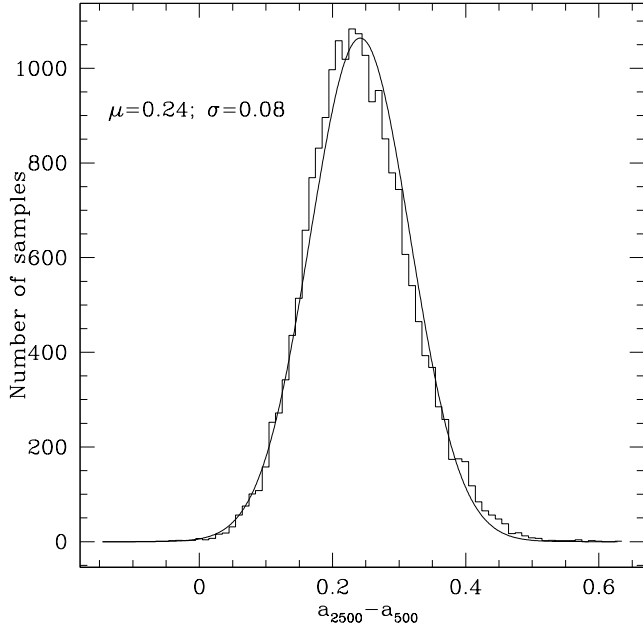


Figure 3. The histogram shows the probability distribution of the difference between M_x/M_L measured at r_{2500} and M_x/M_L measured at r_{500} . The difference is positive at 3σ significance. For comparison, we plot a normal distribution with $\mu = 0.24$, $\sigma = 0.08$.

4 POTENTIAL BIASES

As discussed above, we interpret the change in M_X/M_L with overdensity Δ as evidence of a deviation from hydrostatic equilibrium. However, an obvious concern is whether the result can be explained by biases in our measurements. After all, the geometries of real clusters are more complicated than assumed here (although the ensemble averaged system should be close to spherical). In this section we focus on a number of potential effects that could lead to a radial dependence. Note that other effects can change M_X/M_L , but do so independent of scale; for instance a change in the mean source redshift simply changes all M_Δ 's by the same factor.

4.1 Elongation Bias

An explanation of our results could be that we are introducing a systematic bias through spherical modeling of what we know ought to be triaxial systems. Piffaretti et al. (2003) consider this question in detail. They find that for a broad distribution of elongations and inclinations, the differences between triaxial and spherical X-ray mass estimates are negligible, of order 3%. This fraction is much smaller than the effect we observe. For clusters elongated nearly exactly along the line of sight, Piffaretti et al. (2003) do find that assuming spherical symmetry causes the projected X-ray mass to be underestimated by up to 30% at r_{500} . It is conceivable that through X-ray selection, a number of clusters in our samples might be preferentially elongated close to the line of sight. However, even if present, such elongations cannot reproduce the trend we observe. As Piffaretti et al. (2003) show, geometries that yield a 30% projected mass deficit at r_{500} ought to show a similar deficit at r_{2500} , which we do not observe. Thus while the overall normalization of the

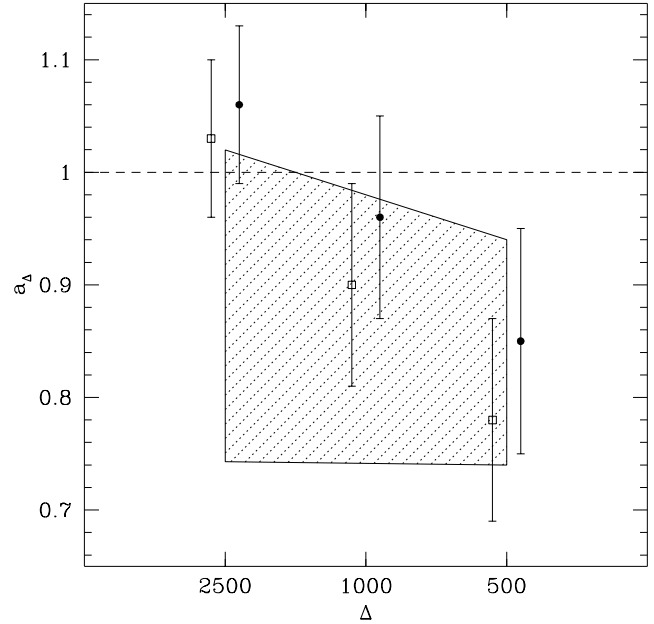


Figure 4. The M_X/M_L ratio as a function of overdensity Δ . The unfilled squares show the data before correction for excess structure along the line of sight as described by Johnston et al. (2007); the filled circles show the data after correction for the effect. The trend is consistent with the X-ray mass underestimate predicted by N-body work (shaded region, Nagai et al. 2007).

trend in Figure 4 might be affected by preferential selection of elongated objects, the trend itself cannot be.

4.2 Extrapolation Bias

We also investigate whether the fact that most $M_{500,X}$ are extrapolated could affect the results. The four clusters for which no X-ray mass extrapolations are necessary are MS 0016, MS 1455, MS 1512, and MS 1621. For these clusters alone, we find $a_{2500} = 0.83 \pm 0.13$, and $a_{500} = 0.61 \pm 0.13$. The difference in these ratios is similar to that of the full sample. Thus there is no indication that the substantial difference between a_{2500} and a_{500} is caused by the extrapolation of the X-ray masses. For the extrapolated sample only, we obtain $a_{2500} = 1.07 \pm 0.08$ and $a_{500} = 0.84 \pm 0.11$. Thus the overall ratios for the extrapolated and unextrapolated subsamples do not differ significantly (the subsamples are uncorrelated, and thus at fixed Δ we can fairly compare the nominal errors in a_Δ for the extrapolated and unextrapolated subsamples).

4.3 Dependence on the Mass-Concentration Relation

We check whether our use of the Bullock et al. (2001) mass-concentration relation to deproject the weak lensing masses could cause the observed trend. We vary the normalization and redshift dependence of the mass-concentration relation. The corresponding mean concentration varies by $\sim 30\%$ (which we note is a rather extreme change), which leads to a systematic variation in the $M_{2500,L}/M_{500,L}$ ratio less than 5%. More recent N-body work shows that the slope of the mass-concentration relation may be somewhat shallower than the Bullock et al. (2001) value (e.g. Neto et al.

2007). However, because our sample spans only an order of magnitude in mass, the effect of changing the slope to the Neto et al. (2007) value (-0.1) is negligible. We therefore conclude that the use of an incorrect NFW concentration cannot reproduce a result of the strength we observe.

4.4 Two-Halo Term Correction

Finally, we consider the possibility that deprojections of weak lensing mass measurements *in general* are biased. When considering the accuracy of weak lensing masses at better than the 20% level, an important effect is the contribution of nearby large scale structure to the weak lensing mass². The recent detection of a “two-halo term”—excess mass due to halos and uncollapsed material outside the virial radius—in Sloan Digital Sky Survey (SDSS) clusters (Johnston et al. 2007) provides direct observational evidence for considering such a contribution.

The “two-halo” term could be an important effect in our measurements. We have carried out the deprojection of the weak lensing masses assuming that they are described by an NFW profile. However, in Johnston et al. (2007) SDSS data, shear measurements out to 30 Mpc indicate that outside the virial radius, the matter density profile gradually flattens. For the range of masses we consider, the Johnston et al. (2007) “two-halo” density profile is very approximately represented by the form

$$\rho_{2H} \propto \frac{1 + (0.25r/r_{200})^2}{r(r_{200} + cr)^2} \quad (7)$$

The above equation resembles an NFW profile within r_{200} , but acquires a flatter r^{-1} shape outside $4r_{200}$. The profile is truncated at 30 Mpc, near where the cluster-mass correlation function becomes negligible (Hayashi & White 2007).

If equation 7 describes the correct density profile, and yet we mistakenly use an NFW profile to deproject the lensing mass, then our 3D mass estimates would exceed the true value. It is straightforward to calculate exactly how much we would overestimate the masses; we can project both the NFW and the “two-halo” profile along the line of sight, and take the ratio of the estimated NFW and “two-halo” 3D masses. This ratio then represents a correction that we can apply to our data on a case-by-case basis. The results appear in Figure 4. We find that while the two-halo term correction does not remove the trend in a_Δ , it does mitigate it, particularly with regards to the large deficit seen at r_{500} .

The M_X/M_L trend remains because any extraneous mass along the line of sight affects mass estimates at all radii, and the difference between the excess at r_{2500} and r_{500} is not sufficient to remove the radial trend in the uncorrected data. The corrected values are $a_{2500} = 1.06 \pm 0.07$, $a_{1000} = 0.96 \pm 0.09$, and $a_{500} = 0.85 \pm 0.10$. If we repeat the bootstrap procedure in Section 3.1, we find that the difference between a_{2500} and a_{500} is reduced to 0.20 ± 0.08 , still significant at 2.5σ , i.e. better than the 98% confidence level.

² As opposed to distant large scale structure which is a source of random noise and not a bias (Hoekstra 2001).

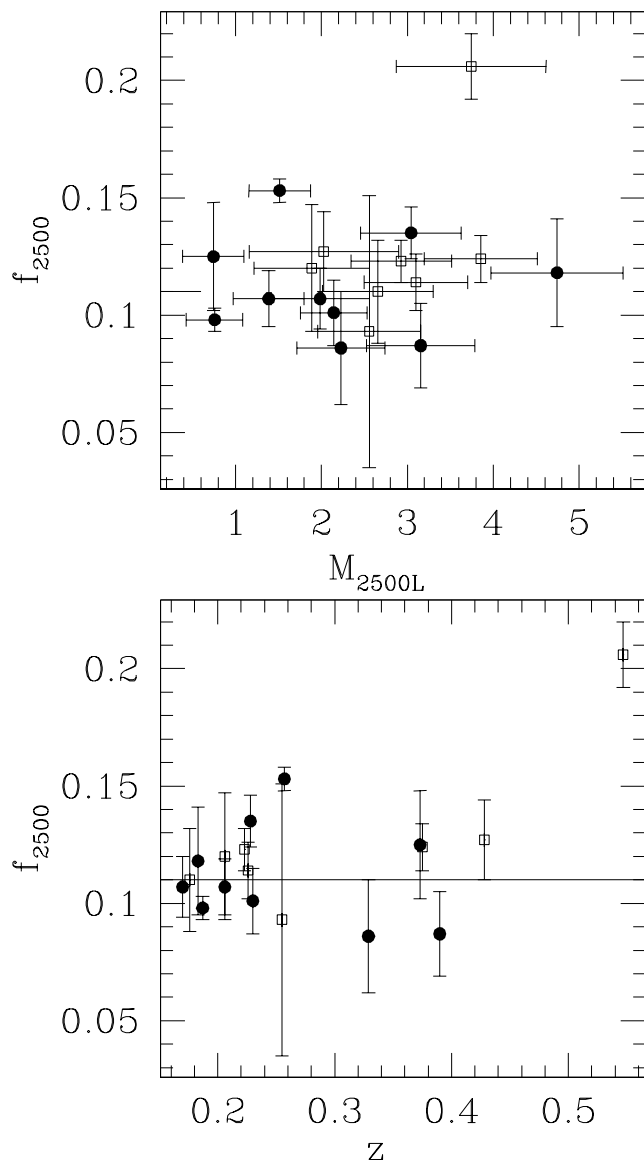


Figure 5. The X-ray gas fraction as a function of (*top*) weak lensing mass at r_{2500} and (*bottom*) redshift. There is no evidence of a trend with mass or redshift. Filled circles and unfilled squares show systems with and without cool cores, respectively. The solid horizontal line shows the Allen et al. (2007) value.

5 GAS FRACTION TRENDS

We also consider the X-ray gas fraction f_{gas} as a function of lensing mass. The gas fraction is an important quantity for cosmology with clusters of galaxies. Under the assumption that f_{gas} approaches a universal value at large enough radii, it is possible to derive constraints on the dark energy equation of state (see Allen et al. 2007, and references therein). The constraints depend crucially on the assumption of universality; if f_{gas} were not a universal number independent of mass and redshift, the dark energy constraints would not be correct (e.g. Vikhlinin et al. 2006).

In Figure 5 we show the X-ray gas fraction as a function of the lensing mass at r_{2500} . There is remarkably little scatter in the relation. The clearest outlier in f_{gas} is MS 0015.9, a previously known high f_{gas} system with triaxial structure

elongated along the line of sight (Piffaretti et al. 2003). Otherwise, the gas fractions are closely clustered around 0.1. The mean value for all systems is $\langle f_{2500} \rangle = 0.119 \pm 0.006$. This value is in excellent agreement with the value found by Allen et al. (2007) for 42 clusters, $f_{2500} = 0.110 \pm 0.002$.

Importantly, f_{2500} is uncorrelated with both $M_{2500,L}$ and z (Kendall's τ is 0.079 and 0.217, respectively). We therefore cannot reject the hypothesis that f_{2500} is independent of lensing mass and redshift.

6 CONCLUSION

We provide a comparison of hydrostatic X-ray and weak lensing masses for a sample of 18 galaxy clusters. What makes our analysis unique is the uniform analysis of Chandra X-ray data and CFHT weak lensing data. This significantly improves the reliability of the comparison. At r_{2500} we find excellent agreement between lensing and X-ray masses: we obtain a ratio $M_X/M_L = 1.03 \pm 0.07$. Interestingly, we observe a significant decrease in this ratio towards larger radii. At r_{500} the ratio is $M_X/M_L = 0.78 \pm 0.09$. Accounting for correlations between the mass measurements, we find that the difference in the ratios is 0.24 ± 0.08 , significant at 3σ . The trend of M_X/M_L with radius is consistent with previous measurements of the $M_L - T$ relation, and is not caused by the assumption of spherical symmetry, extrapolation beyond the Chandra field of view, or uncertainty in the mass-concentration relation.

The trend remains even after we correct for a systematic overestimate of the weak lensing mass due to correlated large scale structure. We show that the trend is consistent with simulations in which nonthermal pressure support causes a systematic underestimate of the cluster mass. Interestingly, the underestimate is not correlated with the presence or absence of a cool core. These results are relevant for upcoming surveys that aim to measure the cosmological parameters from large cluster samples, especially for observations seeking measurements closer to r_{500} .

We also determine the X-ray gas fraction at r_{2500} ; this quantity has been used in several studies to measure w , the parameter of the dark energy equation of state. We find that f_{2500} is not correlated with lensing mass or redshift.

We thank Gus Evrard and Andrey Kravtsov for enlightening discussions. AB and HH acknowledge support from NSERC. AB also acknowledges support from the Leverhulme trust in the form of a visiting professorship at Oxford and Durham Universities. HH also acknowledges support from the Canadian Institute for Advanced Research and grants from NSERC, CFI and BCKDF. This work was partially supported by NASA grant NNX07AE73G. Additional research funding was provided by J. Criswick.

REFERENCES

Allen S. W., 1998, MNRAS, 296, 392
 Allen S. W., Fabian A. C., Kneib J. P., 1996, MNRAS, 279, 615
 Allen S. W., Rapetti D. A., Schmidt R. W., Ebeling H., Morris G., Fabian A. C., 2007, ArXiv e-prints, 706

Allen S. W., Schmidt R. W., Fabian A. C., 2002, MNRAS, 335, 256
 Ameglio S., Borgani S., Pierpaoli E., Dolag K., 2007, ArXiv e-prints, 708
 Balogh M. L., Babul A., Voit G. M., McCarthy I. G., Jones L. R., Lewis G. F., Ebeling H., 2006, MNRAS, 366, 624
 Benjamin J., Heymans C., Semboloni E., van Waerbeke L., Hoekstra H., Erben T., Gladders M. D., Hettterscheidt M., Mellier Y., Yee H. K. C., 2007, MNRAS, pp 820+
 Bullock J. S., Kolatt T. S., Sigad Y., Somerville R. S., Kravtsov A. V., Klypin A. A., Primack J. R., Dekel A., 2001, MNRAS, 321, 559
 Burns J. O., Hallman E. J., Gantner B., Motl P. M., Norman M. L., 2007, ArXiv e-prints 0708.1954, 708
 Cypriano E. S., Sodré L. J., Kneib J.-P., Campusano L. E., 2004, ApJ, 613, 95
 Dickey J. M., Lockman F. J., 1990, ARA&A, 28, 215
 Dolag K., Vazza F., Brunetti G., Tormen G., 2005, MNRAS, 364, 753
 Ettori S., Lombardi M., 2003, A&A, 398, L5
 Evrard A. E., 1990, ApJ, 363, 349
 Faltenbacher A., Kravtsov A. V., Nagai D., Gottlöber S., 2005, MNRAS, 358, 139
 Fernández-Soto A., Lanzetta K. M., Yahil A., 1999, ApJ, 513, 34
 Hallman E. J., Motl P. M., Burns J. O., Norman M. L., 2006, ApJ, 648, 852
 Hayashi E., White S. D. M., 2007, ArXiv e-prints, 709
 Hicks A. K., Ellingson E., Hoekstra H., Yee H. K. C., 2006, ApJ, 652, 232
 Hoekstra H., 2001, A&A, 370, 743
 Hoekstra H., 2007, MNRAS, 379, 317
 Hoekstra H., Yee H. K. C., Gladders M. D., 2002, ApJ, 577, 595
 Ilbert O., Arnouts S., McCracken H. J., Bolzonella M., Bertin E., Le Fèvre O., Mellier Y., Zamorani G., Pellò R., Iovino A., Tresse L., Le Brun V., Rizzo D., Vergani D., 2006, A&A, 457, 841
 Jeltama T. E., Hallman E. J., Burns J. O., Motl P. M., 2007, ArXiv e-prints 0708.1518, 708
 Johnston D. E., Sheldon E. S., Wechsler R. H., Rozo E., Koester B. P., Frieman J. A., McKay T. A., Evrard A. E., Becker M. R., Annis J., 2007, ArXiv e-prints, 709
 LaRoque S. J., Bonamente M., Carlstrom J. E., Joy M. K., Nagai D., Reese E. D., Dawson K. S., 2006, ApJ, 652, 917
 Lima M., Hu W., 2005, Phys. Rev. D, 72, 043006
 Mahdavi A., Hoekstra H., Babul A., Sievers J., Myers S. T., Henry J. P., 2007, ApJ, 664, 162
 Miralda-Escude J., Babul A., 1995, ApJ, 449, 18
 Nagai D., Vikhlinin A., Kravtsov A. V., 2007, ApJ, 655, 98
 Navarro J. F., Frenk C. S., White S. D. M., 1997, ApJ, 490, 493
 Neto A. F., Gao L., Bett P., Cole S., Navarro J. F., Frenk C. S., White S. D. M., Springel V., Jenkins A., 2007, MNRAS, 381, 1450
 Pedersen K., Dahle H., 2007, ApJ, 667, 26
 Piffaretti R., Jetzer P., Schindler S., 2003, A&A, 398, 41
 Poole G. B., Babul A., McCarthy I. G., Fardal M. A., Bildfell C. J., Quinn T., Mahdavi A., 2007, MNRAS, 380, 437
 Poole G. B., Fardal M. A., Babul A., McCarthy I. G., Quinn T., Wadsley J., 2006, MNRAS, 373, 881
 Press W. H., Teukolsky S. A., Vetterling W. T., Flan-

- nery B. P., 1992, Numerical recipes in FORTRAN. The art of scientific computing. Cambridge: University Press, —c1992, 2nd ed.
- Rasia E., Etori S., Moscardini L., Mazzotta P., Borgani S., Dolag K., Tormen G., Cheng L. M., Diaferio A., 2006, MNRAS, 369, 2013
- Sehgal N., Hughes J. P., Wittman D., Margoniner V., Tyson J. A., Gee P., Dell’Antonio I., 2008, ApJ, 672
- Smith G. P., Kneib J., Ebeling H., Czoske O., Smail I., 2001, ApJ, 552, 493
- Squires G., Kaiser N., Babul A., Fahlman G., Woods D., Neumann D. M., Boehringer H., 1996, ApJ, 461, 572
- Squires G., Neumann D. M., Kaiser N., Arnaud M., Babul A., Boehringer H., Fahlman G., Woods D., 1997, ApJ, 482, 648
- Vikhlinin A., 2006, ApJ, 640, 710
- Vikhlinin A., Kravtsov A., Forman W., Jones C., Markevitch M., Murray S. S., Van Speybroeck L., 2006, ApJ, 640, 691